

# Estimation of Peak Wind Force Coefficients Acting on Domed Free Roofs Based on the Quasi-Steady Theory

Yasushi Uematsu<sup>1</sup> and Wei Ding<sup>2</sup>

1. New Industry Creation Hatchery Center, Tohoku University, Sendai 980-8579, Japan

2. National Institute of Technology, Akita College, Akita 011-8511, Japan

**Abstract:** The present paper investigates the methods for estimating the maximum (positive) and the minimum (negative) peak wind force coefficients on domed free roofs based on the quasi-steady theory and the peak factor method, in which the experimental results obtained from our previous studies (2019, 2025) are used. Focus is on the distributions of the peak wind force coefficients along the centerline parallel to the wind direction considering that domed free roof is an axisymmetric body. Empirical formulas are provided to the distributions of mean wind force coefficient, RMS (root mean square) fluctuating wind force coefficient and peak factors as a function of the rise/span ratio of the roof and the turbulence intensity of the approach flow in the along-wind direction at the mean roof height. The proposed methods are validated by the experimental results for the peak wind force coefficients. The methods would provide useful information to structural engineers when estimating the design wind loads on cladding/components of domed free roofs.

**Key words:** Domed free roof, peak wind force coefficient, quasi-steady theory, peak factor, wind tunnel experiment.

## 1. Introduction

Free-standing canopy roofs (or simply free roofs) of various shapes are widely used for structures providing shade and weather protection in public spaces such as parks (see Fig. 1). The roof is usually supported by only columns and therefore wind action is directly exerted on both the top and bottom surfaces of the roof. Being lightweight and flexible, they are vulnerable to dynamic wind actions. Therefore, wind resistance is one of the most important technological problems for structural engineers when designing these roofs.

Regarding planar free roofs, such as gable and mono-sloped roofs, several systematic studies were made (e.g., Gumley [1], Letchford and Ginger [2], Ginger and Letchford [3], Uematsu et al. [4, 5] and Natalini et al. [6]), and the wind force coefficients on these roofs are specified in codes and standards (e.g., ASCE/SEI (American Society of Civil Engineers) 7-22 [7], AS/NZ (Australian and New Zealand Standard) [8] and AIJ (Architectural Institute of Japan) [9]). By comparison, the number of

studies of wind loading on curved free roofs is limited. This is due to difficulties in making wind tunnel models and measuring wind pressures on both the top and bottom surfaces of the roof at many locations. Many pressure taps are required to obtain detailed wind pressure distributions. However, the more pressure taps, the greater the thickness of the roof and the columns because of the tubes inside. As a result, the flow around the roof will be distorted [1]. Natalini et al. [10], Pagnini et al. [11], Uematsu and Yamamura [12], Ding and Uematsu [13] and Ding et al. [14] investigated the wind forces on vaulted free roofs in wind tunnels. HP (hyperbolic paraboloid) is often used for free roofs composed of membranes. The AS/NZ [8] specifies the net wind pressure coefficients for HP-shaped free roofs. However, both the sag/span and rise/span ratios are limited to small values. Wind loads on HP-shaped free roofs were experimentally investigated by several researchers (e.g., Colliers et al. [15], Uematsu et al. [16, 17], and Sun et al. [18, 19]).

---

**Corresponding author:** Yasushi Uematsu, Dr. Eng., specially appointed professor, research fields: wind engineering, snow engineering, structural engineering and steel structure.



**Fig. 1** An example of domed free roof (provided by Taiyo Kogyo Corporation).

Recently, advanced manufacturing techniques such as 3D printers are used to produce wind tunnel models of these roofs [15-17].

To our best knowledge, wind loads on domed free roofs have been investigated by only our research group. Uematsu and Yamamura [20] investigated the design wind loads on domed free roofs based on the results of a wind tunnel experiment, in which they measured the distributions of wind pressures along the centerline parallel to the wind direction. Then, Ding et al. [21] investigated the fundamental characteristics of wind pressures on domed free roofs based on a wind tunnel experiment and a CFD (computational fluid dynamics) analysis using LES (Large Eddy Simulation). They used the same models as those of Uematsu and Yamamura [20]. The flow mechanism causing the characteristic wind pressure distribution for each rise/span ratio was investigated.

The present paper discusses simple methods for estimating the peak wind force coefficients acting on

domed free roofs based on the quasi-steady theory and the peak factor method, in which the results of our previous experiments [20, 21] are employed. We did not conduct another wind tunnel experiment for that purpose. Note that the quasi-steady theory is often used to estimate wind loads for the design of relatively small-scale, rigid structures in building codes and standards of many countries. The results of the present study would provide an important reference to structural engineers when estimating the design wind loads on cladding/components of domed free roofs.

## 2. Outline of Wind Tunnel Experiment

Since the details of the wind tunnel experiment are provided in our previous papers [19, 20], only the outline is shown here.

### 2.1 Wind Tunnel Models

Fig. 2 schematically illustrates the wind tunnel models, which were made by using a 3D printer; the tubing system is installed in the roof and columns. Four models with different rise/span ratios,  $f/D$ , ranging from 0.1 to 0.4 were tested (see Table 1). The geometric scale is assumed to be 1/100. The roof thickness is 2 mm. The mean roof height  $H$  is 80 mm regardless of  $f/D$ . Nine pressure taps of 0.6 mm inside diameter are installed along a centerline both on the top and bottom surfaces, as shown in Fig. 2b. Note that the pressure tap on the bottom surface is 2 mm off the pressure tap on the top surface. Since the spatial variation of wind pressures on the bottom surface is small, the wind

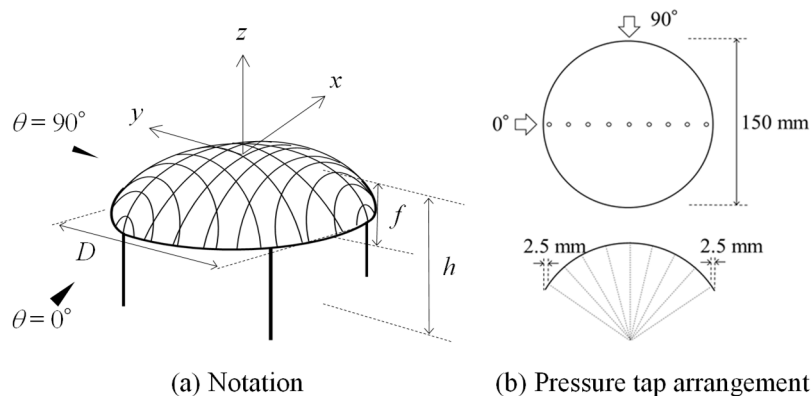


**Fig. 2** Schematic illustration of wind tunnel model.

**Table 1** Dimensions of wind tunnel models.

$f/D$	$f$ (mm)	$D$ (mm)	$h_{\text{top}}$ (mm)	$H$ (mm)
0.1	15	150	88	80
0.2	30	150	95	80
0.3	45	150	103	80
0.4	60	150	118	80

pressure measured at this location is considered to be at the same location as the pressure tap on the upper surface. The roof is supported by four circular columns with an outside diameter of 6.5 mm. It was found that the columns affected the pressures on the bottom surface only slightly [20]. Wind direction  $\theta$  was changed from  $0^\circ$  to  $90^\circ$  at an increment of  $5^\circ$  (Fig. 2), providing the distribution of net wind forces over the whole roof.

### 2.2 Wind Tunnel Flow

The wind tunnel flows in our previous studies [20, 21] were both turbulent boundary layers, which are called Flows 1 and 2, respectively, in this paper. The power-law exponent  $\alpha$  for the mean wind speed profile and the turbulence intensity  $I_{uH}$  in the longitudinal direction at the mean roof height  $H$  were as follows:  $\alpha = 0.21$  and  $I_{uH} = 0.16$  for Flow 1 and  $\alpha = 0.27$  and  $I_{uH} = 0.20$  for Flow 2. The integral scale  $L_x$  of turbulence in the longitudinal direction at a height of 10 cm were approximately 0.2 m for both flows.

### 2.3 Experimental Procedure

The mean wind speed  $U_H$  at the mean roof height  $H$  was set at 9 m/s regardless of  $f/D$ . The velocity scale  $\lambda_V$  was assumed to be 1/2.4, resulting in the time scale of  $\lambda_T (= \lambda_L/\lambda_V) = 1/42$ . The pressure taps were connected to a multi-channel pressure transducer via flexible vinyl tubes of 1 mm internal diameter and 1 m length. Wind pressures at all pressure taps were sampled simultaneously at a rate of 500 Hz for a time duration of 14.3 s, equivalent to 10 min at full scale. The measurements were repeated 10 times for each model. The wind pressure  $P$  is converted to pressure coefficient  $C_p$  as follows:

$$C_p = \frac{P - P_s}{q_H} \quad (1)$$

where  $P_s$  represents the static pressure and  $q_H (= \frac{1}{2}\rho U_H^2$ , with  $\rho$  being the air density) represents the dynamic pressure of approach flow at the mean roof height  $H$ . The wind pressure coefficients on the top and bottom surfaces of the roof are represented by  $C_{pt}$  and  $C_{pb}$ , respectively. The wind force coefficient  $C_f$  is provided by  $C_{pt} - C_{pb}$ . The statistical values of the wind pressure coefficients and wind force coefficients were evaluated by applying ensemble averaging to the results of consecutive 10 runs.

### 3. Estimation of Peak Wind Force Coefficient

In this paper, we discuss simple methods for estimating the peak wind force coefficients using the data presented in Refs. [20] and [21]. If we have the time histories of wind force coefficients  $C_f$ , we can directly estimate the maximum and minimum peak wind force coefficients,  $\hat{C}_f$  and  $\check{C}_f$ . However, in this paper, we discuss simple methods for easily estimating  $\hat{C}_f$  and  $\check{C}_f$  using the data for the mean wind pressure coefficients,  $\bar{C}_{pt}$  and  $\bar{C}_{pb}$ , on the top and bottom surfaces of the roof together with the turbulence intensity  $I_{uH}$  of approach flow in the longitudinal direction at the mean roof height  $H$ . It seems much easier to measure  $\bar{C}_{pt}$  and  $\bar{C}_{pb}$  than to measure  $\hat{C}_f$  and  $\check{C}_f$  in a wind tunnel experiment.

It was found in our previous studies [20, 21] that the contour lines of mean wind force coefficients  $\bar{C}_f$  were nearly perpendicular to the wind direction and the largest values of  $\hat{C}_f$  and  $|\check{C}_f|$  occurred on the centerline parallel to the wind direction. Considering that the domed free roof is an axisymmetric body, we focus on the distribution of wind force coefficient  $C_f$  along the centerline when  $\theta = 0^\circ$ , hereafter.

Using the peak factor method,  $\hat{C}_f$  and  $\check{C}_f$  may be given by the following equations:

$$\hat{C}_f = \bar{C}_f + g^+ \cdot C'_f \quad (2)$$

$$\check{C}_f = \bar{C}_f + g^- \cdot C'_f \quad (3)$$

where  $C'_f$  is the RMS fluctuating wind force

coefficient; and  $g^+$  and  $g^-$  represent the peak factors for  $\hat{C}_f$  and  $\check{C}_f$ , respectively, which are defined by the following equations:

$$g^+ = \frac{\hat{C}_f - \bar{C}_f}{C'_f} \quad (4)$$

$$g^- = \frac{\check{C}_f - \bar{C}_f}{C'_f} \quad (5)$$

Then, using the quasi-steady theory,  $C'_f$  may be provided by the following equation [22]:

$$C'_f = \left\{ 4I_{uH}^2 \bar{C}_f^2 + I_{vH}^2 \left( \frac{\partial \bar{C}_f}{\partial \theta} \right)^2 + I_{wH}^2 \left( \frac{\partial \bar{C}_f}{\partial \phi} \right)^2 \right\}^{1/2} \quad (6)$$

where  $I_{uH}$ ,  $I_{vH}$  and  $I_{wH}$  represent the turbulence intensities at the mean roof height  $H$  in the  $x$ ,  $y$  and  $z$  directions, respectively (regarding the coordinate system, see Fig. 2a). The coordinates  $\theta$  and  $\phi$  are defined as shown in Fig. 3; Point O represents the center of curvature of the roof. Here, we focus on the  $C_f$  distribution along the centerline parallel to the wind direction. Thus, the second term on the right-hand side of Eq. (6) can be ignored, because  $\bar{C}_f$  distribution is symmetric with respect to the centerline.

When  $C_{pt}$  and  $C_{pb}$  are obtained separately using two models with pressure taps either on the top surface or on the bottom surface, as Natalini et al. [10] did, we cannot estimate  $C_f$  directly. In such a case,  $C'_f$  may be provided by the following equation:

$$C'_f = (C_{pt}'^2 + C_{pb}'^2 - 2R_{tb}C_{pt}'C_{pb}')^{1/2} \quad (7)$$

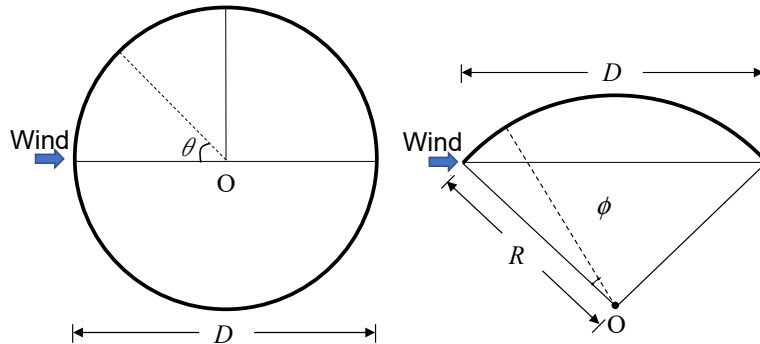


**Fig. 3** Definitions of the coordinates  $\theta$  and  $\phi$ .

where  $C'_{pt}$  and  $C'_{pb}$  are the standard deviations of  $C_{pt}$  and  $C_{pb}$ , respectively; and  $R_{tb}$  is the correlation coefficient between  $C_{pt}$  and  $C_{pb}$ . Since  $R_{tb}$  was not obtained in Refs. [20, 21], it is estimated from  $C'_{pt}$ ,  $C'_{pb}$  and  $C'_f$ , as will be described in the next section.

## 4. Model of Wind Pressure Distribution

### 4.1 Mean Wind Pressure Coefficients

The experimental results for the  $\bar{C}_{pt}$  and  $\bar{C}_{pb}$  distributions along the centerline are shown in Figs. 4 and 5, respectively. In the figures,  $s$  represents the distance from the leading edge to the point of concern along the centerline, normalized by its maximum value  $s_{max}$  for each roof. A detailed discussion of the flow mechanisms causing the  $\bar{C}_{pt}$  and  $\bar{C}_{pb}$  distributions is presented in Ref. [21]. It is found from these figures that the mean wind pressure coefficients are affected by  $I_{uH}$  only a little. The distributions of  $\bar{C}_{pt}$  and  $\bar{C}_{pb}$  can be approximated by the following equation:

$$\bar{C}_\beta = \sum_{i=0}^4 a_i \cos \frac{i\pi s}{s_{max}} \quad (8)$$

where  $\beta$  represents  $pt$  or  $pb$ . The coefficients  $a_i$  can be determined from the data obtained in both Flows 1 and 2 using the least square method. The values of  $a_i$  for  $\bar{C}_{pt}$  and  $\bar{C}_{pb}$  are listed in Table 2. The distribution of  $\bar{C}_f$  ( $= \bar{C}_{pt} - \bar{C}_{pb}$ ) can be obtained from these  $\bar{C}_{pt}$  and  $\bar{C}_{pb}$  distributions.

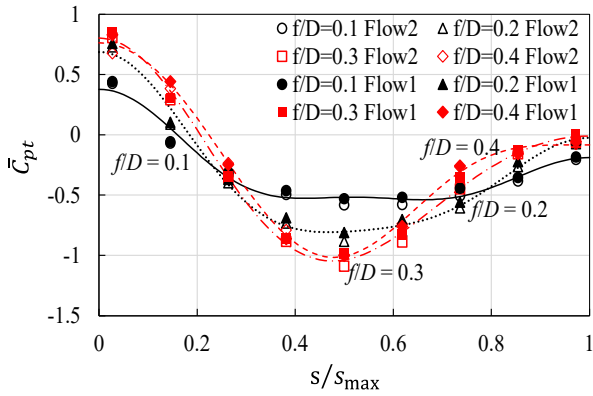


Fig. 4 Distributions of  $\bar{C}_{pt}$  along the centerline.

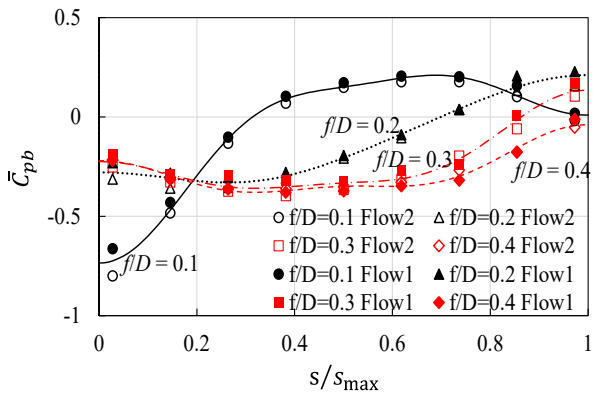


Fig. 5 Distributions of  $\bar{C}_{pb}$  along the centerline.

Table 2 The values of  $a_i$  for  $\bar{C}_{pt}$  and  $\bar{C}_{pb}$ .

$f/D$	$a_0$	$a_1$	$a_2$	$a_3$	$a_4$
0.1	-0.310	0.207	0.306	0.077	0.098
0.2	-0.345	0.251	0.567	0.106	0.108
0.3	-0.329	0.250	0.717	0.156	0.008
0.4	-0.273	0.254	0.673	0.169	-0.061
0.1	-0.040	-0.307	-0.257	-0.066	-0.065
0.2	-0.128	-0.258	0.086	0.013	0.009
0.3	-0.229	-0.145	0.144	-0.035	0.041
0.4	-0.282	-0.074	0.110	-0.017	0.043

#### 4.2 RMS Fluctuating Wind Pressure Coefficients

According to the simplest quasi-steady theory, in which only the  $u$  term in Eq. (6) is considered, the RMS fluctuating wind pressure coefficients,  $C'_{pt}$  and  $C'_{pb}$ , on the top and bottom surfaces of the roof are both proportional to  $I_{uH}$ . Then, the distributions of  $C'_{pt}/I_{uH}$  and  $C'_{pb}/I_{uH}$  along the centerline are plotted in Figs. 6 and 7, respectively. The results indicate that the

$C'_{pt}/I_{uH}$  and  $C'_{pb}/I_{uH}$  values depend on  $I_{uH}$  only slightly. The distributions can be approximated by the following equation like  $\bar{C}_\beta$  (Eq. (8)):

$$C'_\beta = \sum_{i=0}^4 b_i \cos \frac{i\pi s}{s_{\max}} \quad (9)$$

Table 3 summarizes the values of coefficients  $b_i$ , determined from the experimental data in both flows using the least square method.

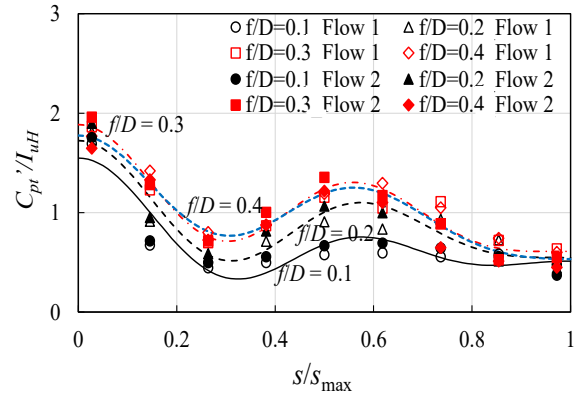


Fig. 6 Distributions of  $C'_{pt}/I_{uH}$  along the centerline.

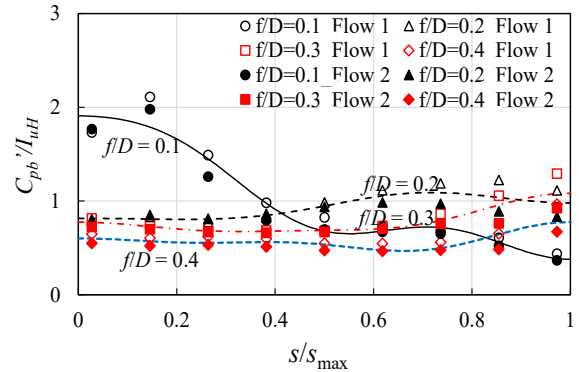


Fig. 7 Distributions of  $C'_{pb}/I_{uH}$  along the centerline.

Table 3 The values of  $b_i$  for  $C'_{pt}$  and  $C'_{pb}$ .

$f/D$	$b_0$	$b_1$	$b_2$	$b_3$	$b_4$
0.1	0.677	0.235	0.175	0.282	0.180
0.2	0.879	0.243	0.065	0.344	0.193
0.3	1.03	0.301	-0.004	0.336	0.213
0.4	1.01	0.315	-0.019	0.306	0.169
0.1	1.01	0.662	0.232	0.102	-0.097
0.2	0.934	-0.140	-0.024	0.058	-0.012
0.3	0.777	-0.121	0.120	-0.033	0.030
0.4	0.572	-0.028	0.076	-0.059	0.040

4.3 Correlation Coefficient between  $C_{pt}$  and  $C_{pb}$

Since  $R_{tb}$  was not obtained in our previous studies [20, 21], we estimate  $R_{tb}$  using the available data for  $C'_f$ ,  $C'_{pt}$  and  $C'_{pb}$ . Figs. 8 and 9 compare the experimental values (circles) of  $C'_f$  with the values estimated from Eq. (7) for various  $R_{tb}$  values (solid lines) when  $f/D = 0.1$  and  $0.2$ , respectively. In practice, the value of  $R_{tb}$  changes with location. However, it is assumed that  $R_{tb}$  is constant over the whole area.

To find the optimal value of  $R_{tb}$ , we computed the mean square error  $E$  defined by the following equation:

$$E = \frac{1}{9} \sum_{i=1}^9 (C'_{fpre,i} - C'_{fexp,i})^2 \quad (10)$$

where  $C'_{fpre,i}$  and  $C'_{fexp,i}$  represent the predicted and experimental values of  $C'_f$  at tap  $i$ , respectively. Fig. 10 shows the variation of  $E$  with  $R_{tb}$  in Flow 2. The value of  $R_{tb}$  providing the minimum value of  $E$  is about  $-0.4$  for  $f/D = 0.1$  and about  $0.2$  for  $f/D = 0.2-0.4$ . These values of  $R_{tb}$  are used for estimating  $C'_f$  using Eq. (7). Fig. 11 compares the experimental results for  $C'_f$  with those estimated from Eq. (7) in Flow 2. A relatively good agreement between experiment and prediction can be seen for all  $f/D$  ratios.

Next, Fig. 12 compares the experimental results for  $C'_f$  with those estimated from Eq. (6) in Flow 2. As mentioned above, the second term on the right-hand side of Eq. (6) can be set to zero. Furthermore, it is assumed that  $I_{wH} = 0.5I_{uH}$  according to Counihan [23] and

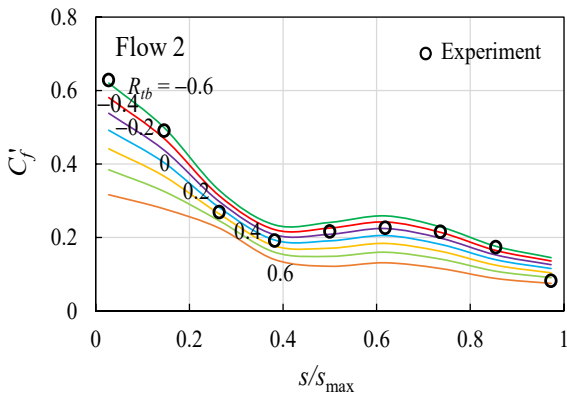


Fig. 8 Distributions of  $C'_f$  along the centerline ( $f/D = 0.1$ ).

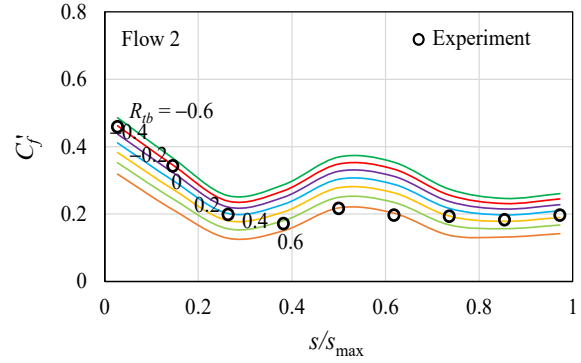


Fig. 9 Distributions of  $C'_f$  along the centerline ( $f/D = 0.2$ ).

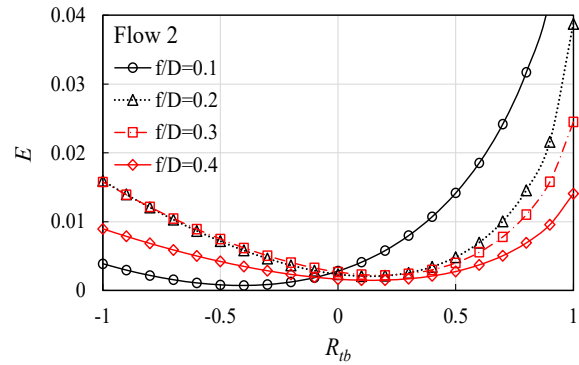


Fig. 10 Variation of  $E$  with  $R_{tb}$  (Flow 2).

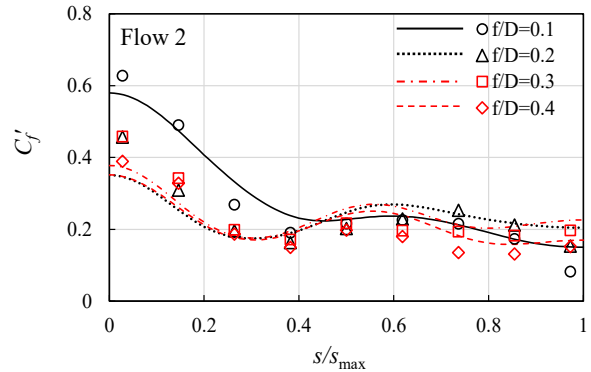


Fig. 11 Comparison of the estimated results using Eq. (7) with the experimental results for the  $C'_f$  distribution (Flow 2).

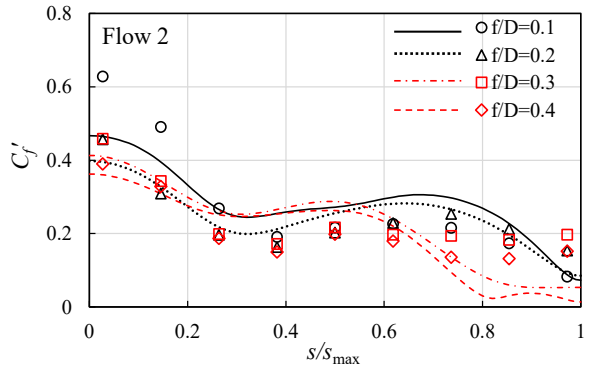


Fig. 12 Comparison of the estimated results using Eq. (6) with the experimental results for the  $C'_f$  distribution (Flow 2).

Teunissen [24]. The fit of the prediction model in Fig. 12 depends on  $f/D$ . Despite the simple prediction model in which only the  $\bar{C}_f$  distribution and  $I_{uH}$  are used, the experimental and predicted values are in relatively good agreement. In particular, the two results are in good agreement over the whole area when  $f/D = 0.2$ . The flow separation from a domed free roof is weaker than that from regular buildings with sharp edges. Therefore, the fluctuating wind forces on domed free roofs are less sensitive to the vortices generated by the flow separation from the structure. In other words, the turbulences in the approach flow may dominate the fluctuating wind forces on domed free roofs.

#### 4.4 Peak Factors

Figs. 13 and 14 show the peak factors,  $g^+$  and  $g^-$ , provided by Eqs. (4) and (5), respectively. Our previous studies [20, 21] revealed that the values of  $\hat{C}_f$  were larger in the windward half area than in the leeward half area. Therefore, the results for  $g^+$  only in the windward half area are considered in Fig. 13. On the other hand, the values of  $\check{C}_f$  were generally large in magnitude in the middle area. Focusing on the  $g^+$  values in the windward area ( $0 < s/s_{\max} < 0.25$ ) where the values of  $\hat{C}_f$  are large and on the  $g^-$  values in the middle area ( $0.25 < s/s_{\max} < 0.75$ ) where the values of  $\check{C}_f$  are large in magnitude,  $g^+$  and  $g^-$  can be approximated by the models as represented by the solid lines in Figs. 13 and 14. The difference between experimental and model values for  $g^+$  is relatively large for  $0.25 < s/s_{\max} < 0.5$ . However, such a difference does not affect the prediction of  $\hat{C}_f$  significantly, because the value of  $\hat{C}_f$  itself is small in this area.

### 5. Prediction of the Maximum and Minimum Peak Wind Force Coefficients

The maximum and minimum peak wind force coefficients,  $\hat{C}_f$  and  $\check{C}_f$ , are predicted by the following two methods and compared with the experimental results.

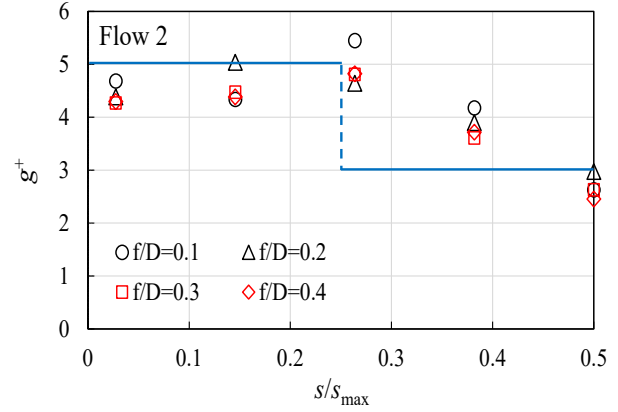


Fig. 13 Distribution of peak factors  $g^+$  (Flow 2).

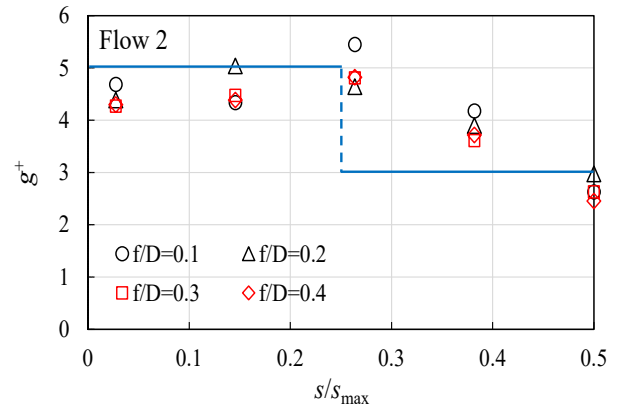


Fig. 14 Distribution of peak factors  $g^-$  (Flow 2).

- Method 1: Empirical formulas for  $\bar{C}_{pt}$  and  $\bar{C}_{pb}$  (Eq. (8), Figs. 4 and 5), Eq. (7), empirical formulas for  $C'_{pt}$  and  $C'_{pb}$  (Eq. (9), Figs. 6 and 7), model of  $R_{tb}$  (Sub-section 4.3), and models of  $g^+$  and  $g^-$  (Figs. 13 and 14) are employed.

- Method 2: Empirical formula for  $\bar{C}_{pt}$  and  $\bar{C}_{pb}$  (Eq. (8), Figs. 4 and 5), Eq. (6), and models of  $g^+$  and  $g^-$  (Figs. 13 and 14) are employed.

Fig. 15 shows comparisons between experiment and prediction by the two methods for the  $\hat{C}_f$  and  $\check{C}_f$  distributions along the centerline in Flow 2 when  $f/B = 0.2$ . And Figs. 16 and 17 show comparisons between experiment and prediction for the  $\hat{C}_f$  and  $\check{C}_f$  values in Flows 1 and 2, in which the results for all models are plotted. The results predicted by the two methods are generally consistent with the experimental ones. Method 1 provides more accurate prediction than Method 2. This is because Method 1 predicts  $C'_f$  more accurately than Method 2. In Method 2,  $C'_f$  is

predicted only from the  $\bar{C}_f$  distribution. Therefore, this method may underestimate the  $C'_f$  values where the magnitude of  $|\bar{C}_f|$  and  $|\partial\bar{C}_f/\partial\phi|$  is small. However, such an underestimation of  $C'_f$  is not a problem in practical design of the cladding/components of domed free roofs because the values of  $\check{C}_f$  are generally small in magnitude in this area. If we focus on the region where the  $\hat{C}_f$  and  $\check{C}_f$  are large in magnitude, the predicted values are in the range of about  $\pm 15\%$  of the experimental ones. In practical design of the cladding/components of domed free roofs, the materials and design specifications do not vary by location and are determined mainly based on the maximum values of  $\hat{C}_f$  and  $|\check{C}_f|$  over the whole area. Therefore, it is said that not only Method 1 but also Method 2 are practical despite the simple models.

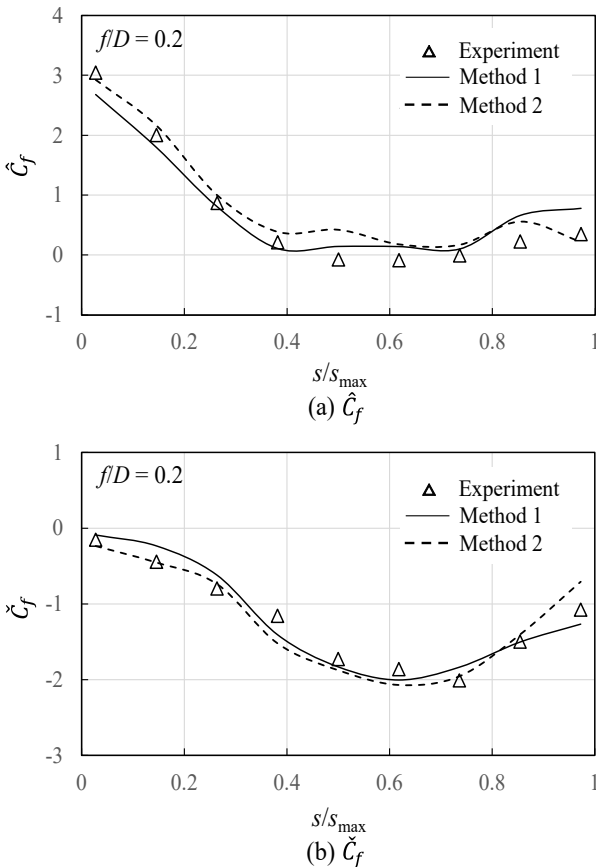


Fig. 15 Comparison between experiment and prediction for the distributions of  $\hat{C}_f$  and  $\check{C}_f$  along the centerline ( $f/D = 0.2$ , Flow 2).

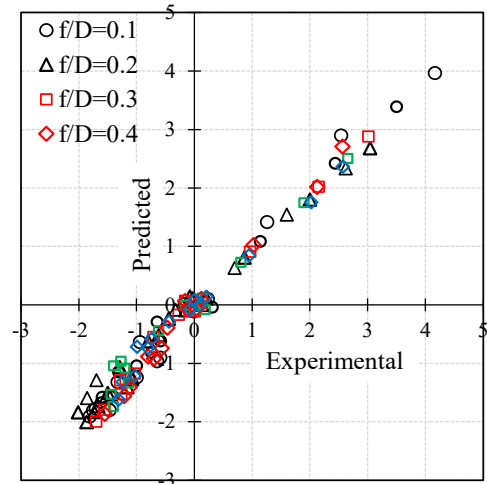


Fig. 16 Comparison for  $\hat{C}_f$  and  $\check{C}_f$  between experiment and prediction by Method 1.

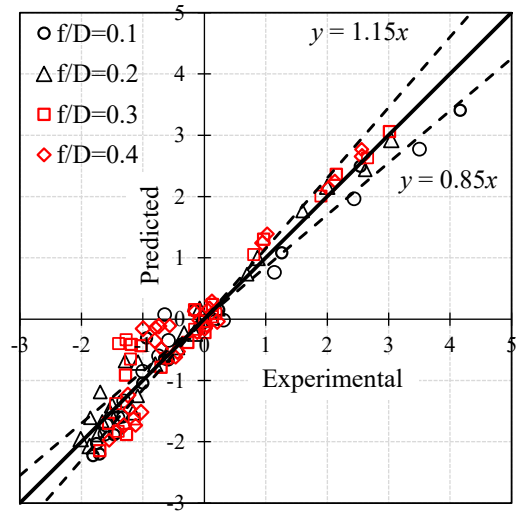


Fig. 17 Comparison for  $\hat{C}_f$  and  $\check{C}_f$  between experiment and prediction by Method 2.

### 6. Concluding Remarks

The present paper discusses simple methods for estimating the maximum and minimum wind force coefficients,  $\hat{C}_f$  and  $\check{C}_f$ , on domed free roofs, based on the available data obtained from our previous studies [20, 21]. Focus is on the distributions of wind pressures along the centerline parallel to the wind direction, because the maximum and minimum peak wind force coefficients on the whole roof occur on this centerline. Empirical formulas were provided to the mean and RMS fluctuating wind pressure coefficients on the top and bottom surfaces of the roof, the

coefficients of correlation between wind pressures on the top and bottom surfaces, and the peak factors for the maximum and minimum peak wind force coefficients. Two methods for estimating the distributions of the maximum and minimum peak wind force coefficients using these empirical formulas were proposed as a function of the rise/span ratio  $f/D$  and the turbulence intensity  $I_{uH}$  in the longitudinal direction of the approach flow at the mean roof height  $H$ , based on the quasi-steady theory and the peak factor method. The validity of the proposed methods was confirmed by the comparison of the predicted results with the experimental ones for  $\hat{C}_f$  and  $\check{C}_f$ .

The present paper would provide useful information to structural engineers when estimating the design wind loads on cladding/components of domed free roofs. However, the experimental conditions in our previous studies [20, 21] were limited. For example, the turbulence intensity  $I_{uH}$  ranged from 0.16 to 0.20, which correspond to Terrain Category II (open country) or III (suburban) specified in the AIJ Recommendations for Loads on Buildings [9]. In such a case the RMS fluctuating wind force coefficients  $C'_f$  are approximately proportional to  $I_{uH}$ . In more turbulent flows, this assumption does not hold due to nonlinear effects.

In our previous study [20], a CFD analysis using LES was also employed. It was found that the CFD analysis provided more detailed results for the mean wind force coefficients  $\bar{C}_f$ . While it is difficult to obtain wind force coefficients at many locations on the roof in wind tunnel experiments, detailed distributions of wind force coefficients can be obtained by CFD analysis. Therefore, CFD analysis would be very useful for estimating  $\hat{C}_f$  and  $\check{C}_f$ . This is the subject of our future studies.

## References

- [1] Gumley, S. J. 1984. "A Parametric Study of Extreme Pressures for the Static Design of Canopy Structures." *Journal of Wind Engineering and Industrial Aerodynamics* 16: 43-56.
- [2] Letchford, C. W., and Ginger, J. D. 1992. "Wind Loads on Planar Canopy Roofs, Part 1: Mean Pressure Distributions." *Journal of Wind Engineering and Industrial Aerodynamics* 45: 25-45.
- [3] Ginger, J. D., and Letchford, C. W. 1994. "Wind Loads on Planar Canopy Roofs, Part 2: Fluctuating Pressure Distributions and Correlations." *Journal of Wind Engineering and Industrial Aerodynamics* 51: 353-70.
- [4] Uematsu, Y., Stathopoulos, T., and Iizumi, E. 2008. "Wind Loads on Free-Standing Canopy Roofs: Part 1 Local Wind Pressures." *Journal of Wind Engineering and Industrial Aerodynamics* 96: 1015-28.
- [5] Uematsu, Y., Stathopoulos, T., and Iizumi, E. 2008. "Wind Loads on Free-Standing Canopy Roofs: Part 2 Overall Wind Forces." *Journal of Wind Engineering and Industrial Aerodynamics* 96: 1029-42.
- [6] Natalini, B., Marighetti, J. O., and Natalini, M. B. 2002. "Wind Tunnel Modeling of Mean Pressures on Planar Canopy Roof." *Journal of Wind Engineering and Industrial Aerodynamics* 90: 427-39.
- [7] American Society of Civil Engineers. 2022. *Minimum Design Loads and Associated Criteria for Buildings and Other Structures*. Reston, VA, USA: ASCE/SEI 7-22.
- [8] Standards New Zealand; Standards Australia. 2021. *Australia/New Zealand Standard: AS/NZ 1170.2*. Wellington, New Zealand: AS/NZ.
- [9] Architectural Institute of Japan. 2015. *Recommendations for Loads on Buildings*. Tokyo: Architectural Institute of Japan.
- [10] Natalini, M. B., Morel, C., and Natalini, B. 2013. "Mean Loads on Vaulted Canopy Roofs." *Journal of Wind Engineering and Industrial Aerodynamics* 119: 102-13.
- [11] Pagnini, L., Torre, S., Freda, A., and Piccardo, G. 2022. "Wind Pressure Measurements on a Vaulted Canopy Roof." *Journal of Wind Engineering and Industrial Aerodynamics* 223: 104934.
- [12] Uematsu, Y., and Yamamura, R. 2019. "Wind Loads for Designing the Main Wind-Force Resisting Systems of Cylindrical Free-Standing Canopy Roofs." *Technical Transactions, Civil Engineering* 7: 124-44.
- [13] Ding, W., and Uematsu, Y. 2022. "Discussion of Design Wind Loads on a Vaulted Free Roof." *Wind* 2: 479-94.
- [14] Ding, W., Uematsu, Y., and Wen, L. 2023. "Fundamental Characteristics of Wind Loading on Vaulted Free Roofs." *Wind* 3: 394-417.
- [15] Colliers, J., Bollaert, M., Degroote, J., and Laet, L. D. 2019. "Prototyping of Thin Shell Wind Tunnel Models to Facilitate Experimental Wind Load Analysis on Curved Canopy Structures." *Journal of Wind Engineering and Industrial Aerodynamics* 188: 308-22.
- [16] Uematsu, Y., Miyamoto, Y., and Gavanski, E. 2014. "Wind Loading on a Hyperbolic Paraboloid Free Roof."

**Estimation of Peak Wind Force Coefficients Acting on Domed Free Roofs  
Based on the Quasi-Steady Theory**

- Journal of Civil Engineering and Architecture* 8 (10): 1-19.
- [17] Uematsu, Y., Miyamoto, Y., and Gavanski, E. 2015. "Effect of Porosity on the Wind Loads on a Hyperbolic Paraboloid Canopy Roof." *Journal of Civil Engineering and Architecture* 9 (6): 715-26.
- [18] Sun, X., Yu, R., and Wu, Y. 2019. "Investigation on Wind Tunnel Experiments of Ridge-Valley Tensile Membrane Structures." *Engineering Structures* 187: 104371.
- [19] Sun, X., Arjun, K., and Wu, Y. 2020. "Investigation on Wind Tunnel Experiment of Oval-Shaped Arch-Supported Membrane Structures." *Journal of Wind Engineering and Industrial Aerodynamics* 206: 104371.
- [20] Uematsu, Y., and Yamamura, R. 2019. "Experimental Study of Wind Loads on Domed Free Roofs." In *Proceedings of the XV Conference of the Italian Association for Wind Engineering*, IN-NENO 2018, Lecture Note in C.E., 27, pp. 716-29.
- [21] Ding, W., Wen, L., and Uematsu, Y. 2025. "Aerodynamic Forces on Domed Free Roofs." In *Proceedings of the 16th International Conference on Wind Engineering*, Florence, Italy, August 27-31, 2023.
- [22] Letchford, C. W., Iverson, R. E., and McDonald, J. R. 1993. "The Application of the Quasi-Steady Theory to Full Scale Measurements on the Texas Tech Building." *Journal of Wind Engineering and Industrial Aerodynamics* 48: 111-32.
- [23] Counihan, J. 1975. "Adiabatic Atmospheric Boundary Layers. A Review and Analysis of Data from the Period 1880-1972." *Atmospheric Environment* 9: 871-905.
- [24] Teunissen, H. W. 1979. "Measurements of Planetary Boundary Layer Wind and Turbulence Characteristics over a Small Suburban Airport." *Journal of Wind Engineering and Industrial Aerodynamics* 4: 1-34.